FULL TITLE
*ASP Conference Series, Vol. **VOLUME**, **YEAR OF PUBLICATION***
NAMES OF EDITORS

Structure and Evolution of Magnetic Fields Leading to Solar Flares

Haimin Wang

Big Bear Solar Observatory, New Jersey Institute of Technology

Abstract. In this paper, I review the observations of preflare magnetic conditions. The following topics will be discussed: (1) Static non-potential magnetic topology before flares, such as high magnetic gradient, strong magnetic shear and large twist and electric current. (2) Dynamic pre-flare conditions such as new flux emergence, helicity injection and shear/converging flows. (3) The evolution of these magnetic structures leading to and following flares. Unprecedented vector magnetograms from Solar-B, with high resolution, cadence, stability, will certainly make breakthroughs in this research area.

1. Static Pre-flare Conditions

It is generally believed that the magnetic field provides the energy for the solar energetic events, e.g., flares, CMEs. Although the details of energy storage and release have not yet fully understood, from the observational point of view, the frequency and intensity of the activity seen in the solar corona correlate well with the size and complexity of the host active region (Sawyer et al. 1986; McIntosh 1990; Falconer et al. 2003). Those active regions of a non-potential configuration (i.e., with significant field-aligned currents) can easily store $10^{30} - 10^{33}$ ergs energy appropriate for powering flares (Krall et al. 1982; Metcalf et al. 1995; Metcalf, Leka & Mickey 2005). Schrijver et al. (2005) classified active regions into flare-active and flare-quite regions according to the comparison of extrapolated 3-D potential magnetic fields and TRACE coronal loops. Flares are found to occur 2.4 times more frequently in active regions with non-potential coronae than in near-potential regions, while their average X-ray peak flare brightness is 3.3 times higher. In an effort to identify an activity-productive indicator, numerous photospheric magnetic properties have been explored. For example, based on 18 years of observations, Zirin and Liggett (1987) found that δ sunspots are responsible for almost all great flares; Wang et al. (1994) examined the temporal variation of the total vertical current in an active region and suggested that the existence of strong current systems contributes to the flare activity. The importance of magnetic share to the flare occurrence was first introduced by the MSFC group (e.g. Hagyard et al., 1984). Kurokawa et al. (1987) pointed out that the shear can be developed by two different ways: collision of two sunspots of opposite magnetic polarities and the successive emergence of twisted magnetic flux ropes. Falconer (2001) measured the length of strong-field, strong-sheared neutral line (LSS) and global net current of four active regions and proposed that they might be prospective predictors of the CME productivity of active

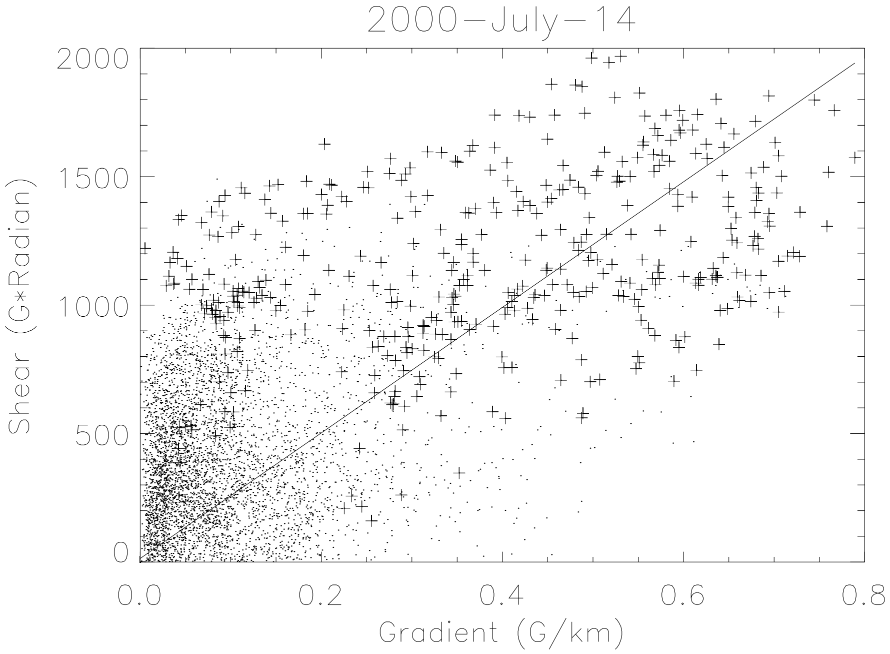

Figure 1. Scatter plot of magnetic shear vs. magnetic gradient in all the points along all the neutral lines identified for the active region 9077 on 2000 July 14. Plus signs are the points along the flare neutral line. The solid straight line is a linear fit of all the data points (Wang et al., 2006).

regions. In addition, Wang et al. (2006) studied the magnetic structure of five active regions that produce great flares and found a positive correlation between the magnetic gradient and magnetic shear. Leka and Barnes (2003a,b) have addressed potential and limitation of using photospheric magnetic field properties to distinguish flare-productive and flare-quite regions.

Figures 1 demonstrates the results of Wang et al. (2006), on the analysis of Bastille day flare July 14, 2000. It shows the scatter plot of magnetic shear as a function of magnetic gradient for all the points along all the magnetic neutral lines in the active region. The plus signs represent points in the section of flaring neutral line. Apparently, these points (plus signs) have both higher magnetic shear and gradient than other points (dots) in the active region. Furthermore, it is evident that there is a positive correlation between magnetic gradient and magnetic shear. Although a large scatter is present in the plot, the linear relationship between the two parameters (gradient and shear) is substantial. The correlation coefficient (C.C.) is 76% if using all the points in the active region. However, if only the points at the flaring neutral line are used, the C.C. increases to 89%.

Naturally, the next step is to establish a more quantitative relationship between flare index and magnetic parameters that reflect magnetic topology of active regions.

The flare productivity of a given active region is assessed by the soft X-ray (SXR) flare index (FI) that was first introduced by Antalova (1996). The FI is defined by weighting the SXR flares of classes B, C, M and X as 0.1, 1, 10 and 100, respectively (in units of $10^{-6} Wm^{-2}$), regardless their duration. The daily FI_{SXR} can be written in the following way (Abramenko 2005):

$$FI_{SXR} = (100 \times \sum_{\tau} S_X + 10 \times \sum_{\tau} S_M + 1 \times \sum_{\tau} S_C + 0.1 \times \sum_{\tau} S_B)/\tau \qquad (1)$$

where τ is the length of time (measured in days) that an active region lasts during its disk passage, $\sum S_X$, $\sum S_M$, $\sum S_C$ and $\sum S_B$ are the GOES peak intensities of X, M, C and B classes produced by this active region for the duration τ. As we shorten the period, the shorter term of daily FI_{SXR} can be derived (such as the daily FI_{SXR} based on the one-day flare activity).

On the other hand, the quantities describing the magnetic complexity and non-potentiality of active regions and under consideration may include (B_x, B_y and B_z are the transverse and the line-of-sight components of the magnetic field in the following discussions):

1. **Horizontal Gradient of the Line-of-sight Magnetic Field**. The magnitude of horizontal gradient of the line-of-sight field quantifies the "sunspot distribution" component of the McIntosh classification (McIntosh 1990) and has generally been thought to be a proxy of flare activity (McIntosh 1990; Zhang et al. 1994; Gallagher, Moon & Wang 2002; Wang et al. 2006).

$$|\nabla_h B_z| = [(\frac{\partial B_z}{\partial x})^2 + (\frac{\partial B_z}{\partial y})^2]^{1/2} \qquad (2)$$

2. **Length of Gradient Neutral Line (GNL)**, i.e., the length of a segment with strong gradient around the magnetic neutral line (Falconer et al. 2003; Song et al. 2006). An gradient threshold 50G/Mm was suggested to determine the quantity by Song et al. (2006).

3. **Median and Mean Value of Gradient around the Neutral Line** .

4. **Line-of-Sight Photospheric Magnetic Energy Dissipation** (Abramenko et al. 2003).

$$\epsilon(B_z) = 4[(\frac{\partial B_z}{\partial x})^2 + (\frac{\partial B_z}{\partial y})^2] + 2(\frac{\partial B_z}{\partial x} + \frac{\partial B_z}{\partial y})^2 \qquad (3)$$

5. **Magnetic Shear Angle**, i.e., the angle between the observed transverse field and the potential transverse field.

6. **Vertical Current Density and Force Free Constant**. It has been hypothesized that the existence of strong current system contributes to the flaring activity (Wang et al. 1994).

$$J_z = (\frac{\partial B_y}{\partial x} - \frac{\partial B_x}{\partial y})/\mu_0 \qquad (4)$$

where μ_0 is the magnetic permeability. Furthermore, the ratio between the current density and B field will give another important parameter: the force free constant α that is often used as a measure of the twist of magnetic fields (Hahn et al., 2005).

7. **Photospheric Excess Magnetic Energy Density**, i.e., the total difference between the observed and the potential fields (Wang et al. 1996; Leka & Barnes 2003a,b). This is not the density of the true free energy because this quantity is computed at the photospheric boundary, not in the coronal volume.
$$\rho_e = (B_p - B_o)^2/8\pi \tag{5}$$
where subscripts o and p refer to observed and potential fields, respectively.

8. **Magnetic Free Energy**. It is quite plausible that the extreme solar activity is powered by the magnetic free energy (Metcalf, Leka & Mickey 2005). Under the assumption that the magnetic field is force-free, the magnetic Virial Theorem (Chandrasekhar & Fermi 1953; Molodenskii 1969) yields the total magnetic energy in the coronal volume. Subtracting the energy of the equivalent potential field, we can derive the free energy in the coronal volume.
$$E_{free} = \int_{z_0} (xB_{xo} + yB_{yo} - xB_{xp} - yB_{yp})B_z \, dxdy \tag{6}$$
where subscripts o and p refer to observed and potential, respectively. z_0 is the observed boundary.

Jing et al. (2006) has obtained some preliminary results to demonstrate the feasibility of establishing the relationship between magnetic topology and flare index quantitatively. They started with the parameters that could be derived directly from the line-of-sight magnetograms, such as the length of GNL, the mean gradient values of the neutral lines and the photospheric magnetic energy dissipation. The data source was the MDI line-of-sight magnetograms, primarily because those data are regularly obtained, extensively archived and free of the atmospheric seeing. They selected 87 active regions, derived the above quantities when the active regions were near the disk center and examined the statistical magnitude scaling correlation with the flare index of the active regions. Sample results are shown in Figure 2. Left panels are based on the flare index for the entire disk passage, while the right panels are for 1 day index, starting from the time of analyzed magnetogam. They noted that, as the correlation between the 1-day flare index and magnetic parameters are evaluated, predictability of flares based on length of GNL and magnetic energy dissipation decreases while that based on mean gradient value increases.

2. Dynamic Pre-flare Conditions

Although the snapshot magnetic field observations can provide quite useful tools to predict likelihood of flares, the dynamic properties of magnetic fields should

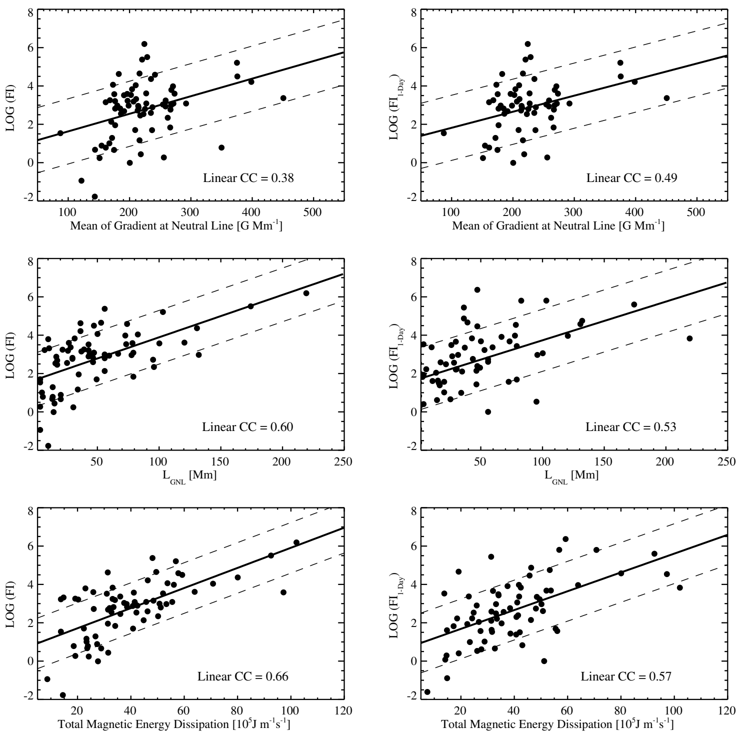

Figure 2. Scatter plots to compare flare index (in the form of logarithm) and magnetic parameters. The left panels are based on flare index of entire disk passages of active regions, right is based on one-day flare index. The magnetic parameters presented from top to bottom are: mean gradient on the magnetic neutral line; length of neutral line with magnetic gradient larger than 50G/Mm; and total magnetic energy dissipation. The solid lines show the least-squares linear fit to the data points. The dashed lines show the interval of the standard deviation at 95% level of confidence (Jing et al., 2006).

provide even broader knowledge of pre-flare conditions. We noted the two important aspects: (1) New flux emergence regions (EFRs) and (2) Flow motions in active regions.

The importance of EFRs leading to solar activities was noted more than two decades ago (e.g., Zirin, 1983). Tanaka (1991) made some fundamental discovery in investigating the complex subsurface magnetic rope structure of a very flare-active isolated δ group. This group showed unusually fast evolution accompanied by a number of intense flares occurring on the neutral line of the δ spot, and made it possible to study the inherent relation of flare occurrence to changes of the magnetic configuration. The evolution of this isolated δ group is shown to decompose into two flare-associated elementary modes: shearing produced by spot growth, and reduction of shear as spots disappear. A model of an emerging twisted magnetic knot was proposed to explain the observed magnetic field evolution. The inferred magnetic topological structure of this

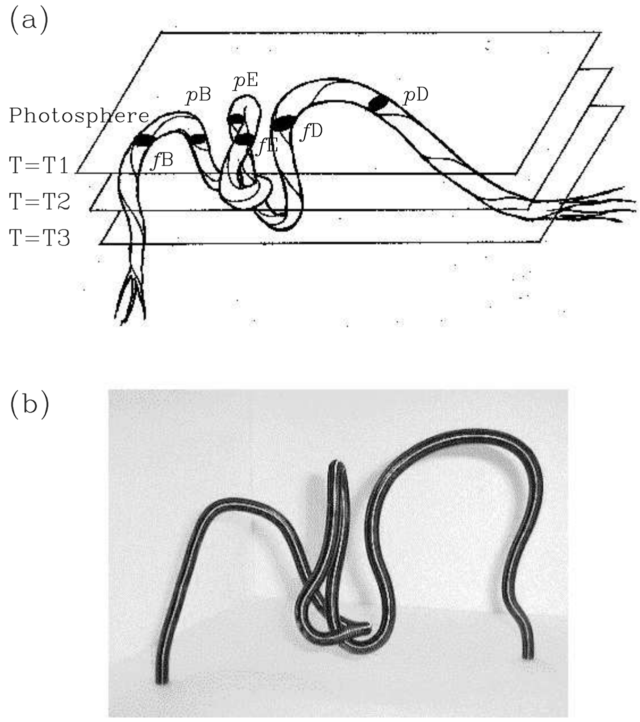

Figure 3. Kurokawa's cartoon model to explain the observed magnetic field evolution of AR 9026 by emergence of twisted flux ropes (Kurokawa et al. 2002).

region consists of tightly twisted knots and a long-winding twisted rope with an internally reversed loop and a hooked bottom structure. The abnormal evolution of this δ group was explained by their consecutive emergences. This concept was further explored by Ishii et al. (1998, 2000) and Kurokawa et al. (2002). In particular Kurokawa et al. (2002) studied the flare-productive AR 9026 for its long-term evolution and found drastic changes in the δ sunspot configuration that started several hours before the big flares of 2000 June 6. In particular, they reported the catastrophic decay of the central δ spot region from 10:00 UT of June 6 to 16:00 UT of June 7. They constructed a schematic model of an emerging twisted flux rope to explain this drastic evolution based on magnetic flux change in the whole active region as shown in Figure 3.

Zirin & Wang (1993) discovered that magnetic flux can emerge inside the penumbrae of existing sunspots. This kind of new flux emergence can produce so-called magnetic channel, which is an elongated magnetic structure with alternating magnetic polarities and strong transverse magnetic fields along the channels (see e.g., Figure 3 of Zirin and Wang (1993)). Surface plasma flows are observed along the channels as well. The penumbral flux emergence is also known to be a common property of a few super-active regions, which produced multiple major solar flares, such as NOAA 5395 in March 1989, NOAA 5629 in August 1989, NOAA 5747 in October 1989 (see Tang and Wang, 1993 for these three regions), NOAA 6659 in June 1991, and NOAA 9393 in March/April 2001.

Very recently, Yang et al. (2004) demonstrated that the power of diffraction limited observations to track flows in active regions that produced flares. They presented high spatial resolution observations of proper motions in the solar NOAA Active Region 10486 using a high-order adaptive optics system, frame selection, and speckle-masking image reconstruction. The data were obtained with the Dunn Solar Telescope of the National Solar Observatory/Sacramento Peak on 2003 October 29. The resolution of the images approaches the diffraction limited of the Dunn Solar Telescope of about $0.14''$ at 527 nm. They analyzed a 2 hr time series with a 1 minute cadence prior to an X10 white-light flare. They found specific evidence of strong shear flows along the magnetic neutral line; these shear flows are well defined and correlated with white-light flare kernels in the visible and infrared. The speed along the flow channels can reach up to 1.6 km/s, and the separation of channels with head-on flows can be less than $1''$. Counterstreaming and complex flow patterns have been distinguishing characteristics of this extraordinarily flare-productive active region. Figure 4 demonstrates a summary of their results.

In a recent study, Maeshiro et al. (2005) found a close correlation between magnetic helicity injection and Soft X-ray activity. Obviously, the helicity injection combines two terms of solar magnetic field evolution, flux emergence and flow motions. Therefore, study of magnetic helicity evolution may lead new insights in understanding the relationship between the evolution of magnetic fields and flares.

3. Rapid Changes of Surface Magnetic Fields As a Result of Flares

Only recently have rapid and permanent changes of photospheric magnetic fields been observed to be associated with large solar flares. Many previous studies generated inconclusive results (Ambastha et al., 1993, Hagyard et al., 1999, Chen et al., 1994, Li et al., 2000a&b). Kosovichev & Zharkova (2001) studied high resolution MDI magnetogram data for the 2000 July 14 "Bastille Day Flare" and found regions with a permanent decrease of the magnetic flux, which were related to the release of magnetic energy. Using 1 minute cadence GONG++ data, Sudol and Harvey (2005) surveyed rapid and permanent changes of line-of-sight magnetic fields that are indeed associated with almost all the X-class flares studied. Earlier, BBSO group published a number of papers describing the sudden appearance of unbalanced magnetic flux that is associated with flares (Spirock et al., et al., 2002; Wang et al., 2002b; Yurchyshyn et al. 2004; Wang et al. 2004b).

Very recently, BBSO group presented a new observational result of rapid changes of sunspot structure associated with a substantial fraction of flares (Wang et al. 2004a; Deng et al. 2005; Liu et al. 2005). In particular, Liu et al. (2005) studied the relationship between the change in δ spot structures and associated major flares for seven events. The results are quite consistent for all the events: part of the penumbral segments in the outer δ spot structure decay rapidly after major flares; meanwhile, the neighboring umbral cores and/or inner penumbral regions become darker. The rapid changes, which can be identified in the time profiles of white-light (WL) mean intensity, are permanent, not transient, and thus are not due to flare emissions. The co-aligned

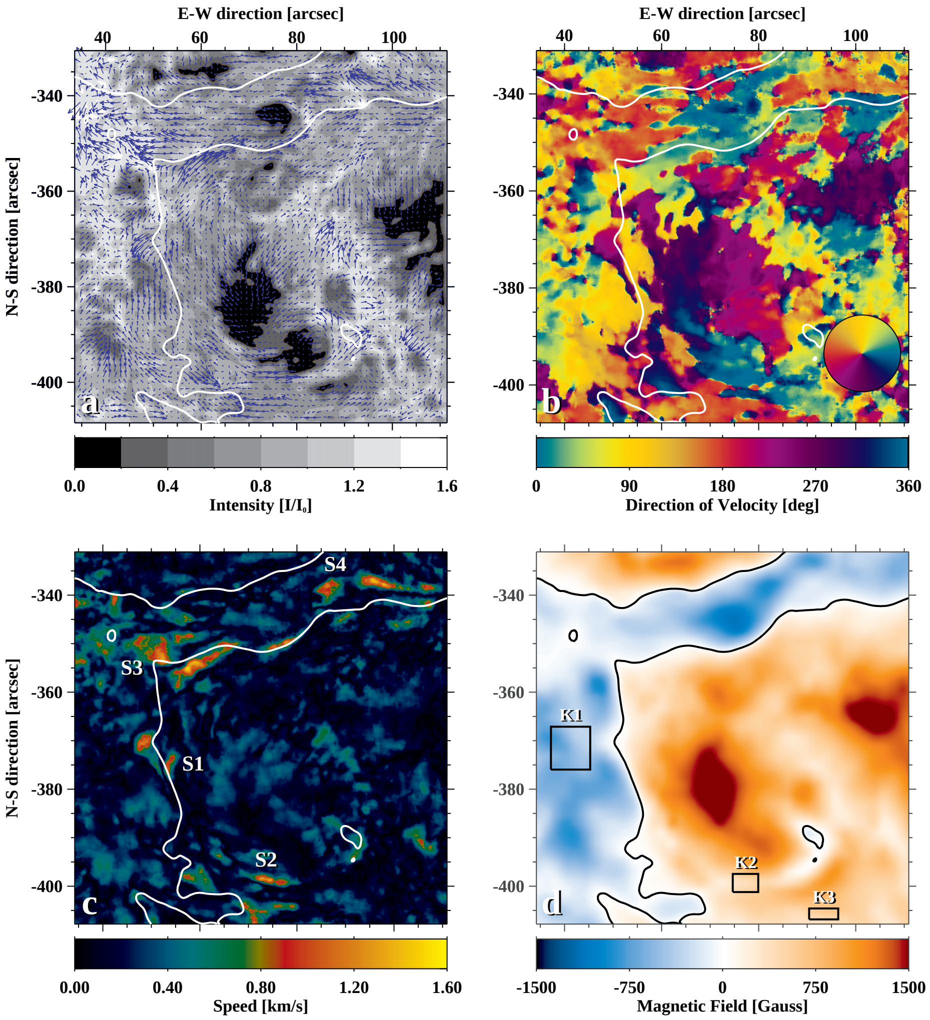

Figure 4. Photospheric flows and magnetic field configuration of NOAA 10486 on 2003 October 29. To illustrate the results of high spatial resolution local correlation tracking analysis of WL data, it provides different views of (a) flow vectors, (b) azimuthal angle of the velocity vectors, (c) magnitude of the velocity vectors, and (d) MDI magnetogram with superimposed magnetic neutral lines. I/I_0 in (a) is the normalized intensity relative to quiet photosphere (Yang et al. 2004).

magnetic field observations show substantial changes in the longitudinal magnetic field associated with the decaying penumbrae and darkened central areas. For two events for which vector magnetograms were available, they find that the transverse field associated with the penumbral decay areas decreased, while it increased in the central darkened regions. Both events also show an increase in the magnetic shear after the flares. For all the events, they find that the locations of penumbral decay are related to flare emission and are connected by prominent TRACE post-flare loops. To explain these observations, they propose a reconnection picture in which the two components of a δ spot become strongly connected after the flare. The penumbral fields change from a highly inclined to a more vertical configuration, which leads to penumbral decay. The umbral core and inner penumbral region become darker as a result of increasing longitudinal and transverse magnetic field components. Figure 5 presents a sample event (2003 October 29 flare).

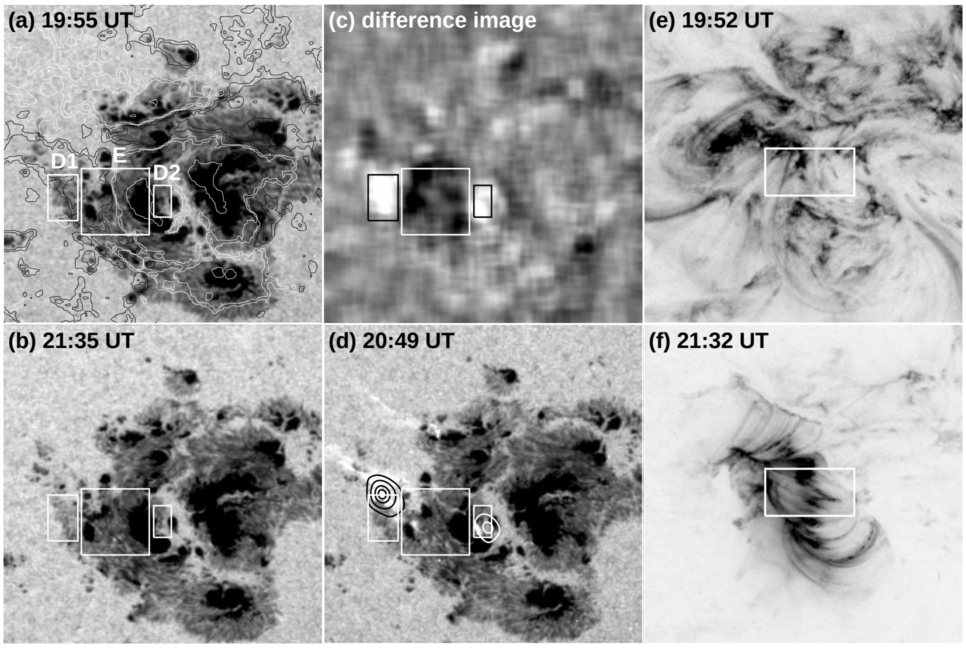

Figure 5. Comparison of preflare (a, e) and postflare (b, f) states for the X10 flare on 2003 October 29. (a, b) and (e, f) are TRACE WL and 195 Å images, respectively. (c) is the WL difference image (the postflare image minus the preflare image). (d) is the WL image at flare maximum with superimposed RHESSI 50–100 keV hard X-ray contours. D1 and D2 are two areas of penumbral decay and E is the region of sunspot enhancement along the neutral line. The white contours in (a) represent the line-of-sight field (Liu et al., 2005).

Finally, let us address a more challenging issue: based on the real-time monitoring of magnetic structure of active regions, can we predict the imminent (say within an hour) occurrence of flare? The observations of magnetic field evolution with one-minute cadence has demonstrated the rapid changes of magnetic structure associated with flares; however, these change immediately followed flares (Wang et al, 2002, Liu et al., 2005, Sudol and Harvey, 2005). Therefore, it is difficult to use them to predict flares. However, based on the work by Stoltz (2005), it may be hopeful to monitor the flow fields and predict the imminent flares.

Figure 6 demonstrates an example (2001 April 6 X5.6 flare in AR 9415) from Stoltz (2005). The top panels of the figure shows that magnetic gradient along magnetic neutral line suddenly enhanced immediately following the flare. Two bottom panels show the relative motion of sunspots of opposite polarities following the flare. In the X direction (normal to the neutral line), converging motion starts immediately following the flare; in the direction along the neutral line, an earthquake-like shear motion was found: before the flare, the two sunspots of opposite polarities in the two sides of the flaring neutral line were undergoing shearing motion. As soon as the flare occurred, the two spots slid back rapidly and reversed the direction of the relative motion. Obviously, this motivates people to include the flow field studies in data analysis along with magnetic field evolution, which may provide another key piece of information to understand the triggering of flares: the rapidly increased shear motion could be the precursor of a flare.

4. Summary

As discussed above, tracking of structure and evolution of magnetic fields may provide important clues about the pre-flare magnetic conditions. The most important vital signs of a flare productive region includes: non-potential magnetic topology, new flux emergence and complicated flow patterns. Obviously, SOT on board Solar-B will provide unprecedented vector magnetograms with highest spatial resolution, polarization sensitivity, cadence and stability. Exciting new results will be anticipated from this upcoming mission.

Acknowledgments. I am grateful to the Solar-B team and Prof. Shibata for inviting me to attend this workshop and give this review. The work is supported by NSF under grants ATM-0313591 and ATM-0536921, NASA under grants NAG5-13661.

References

Ambastha A. Hagyard, M. J. & West E. A., 1993, Sol. Phys., 148, 277
Abramenko, V. I., Yurchyshyn, V. B., Wang, H., Spirock, T. J., & Goode, P. R., 2003, Ap.J., 597, 1135
Abramenko, V. I., 2005, Ap.J., 629, 1141
Amari, T., Luciani, J. F., Aly, J. J., & Tagger, M., 1996, Ap.J. Letters, 466, L39
Antalova, A., 1996, *Daily Soft X-Ray Flare Index (1969=1972)*, Contributions of the Astronomical Observatory Skalnate Pleso, 26, 98
Chandrasekhar, S. & Fermi, E., 1953, Ap.J., 118, 116
Chen, J. Wang, H., Zirin, H. & Ai, G., 1994, Sol. Phys., 154, 261
Deng, N., Liu, C., Yang, G., Wang, H., & Denker C., 2005, Ap.J., 623, 1195
Falconer, D. A., 2001, Journal of Geophysical Research, 106, 25185
Falconer, D. A., Moore, R. L., & Gary, G. A., 2003, Journal of Geophysical Research, 108, SSH 11-1
Gallagher, P., Moon, Y. J., & Wang, H. 2002, Sol. Phys., 209, 171
Hagyard et al., 1984, Sol. Phys., 91, 115
Hagyard et al., 1999, Sol. Phys., 184, 133
Hahn, M., Gaard, S., Jibben, P., Canfield, R.C. and Nandy, D., 2005, Ap.J., 629, 1135
Ishii, T., Kurokawa, H. & Takeuchi, T., 1998, Ap.J., 499, 898
Ishii, T., Kurokawa, H. & Takeuchi, T., 2000, PASJ, 52, 337
Jing, J., Song, H., Abramenko, V.I., Tang, C. & Wang, H., 2006, Ap.J. Letters, to be submitted
Kosovichev, A. G., & Zharkova, V. V., 2001, Ap. J. Letters, 550, L105
Kurokawa, H., 1987, Sol. Phys. 113, 259
Kurokawa, H., Wang, T. & Ishii, T., 2002, Ap.J., 572, 598

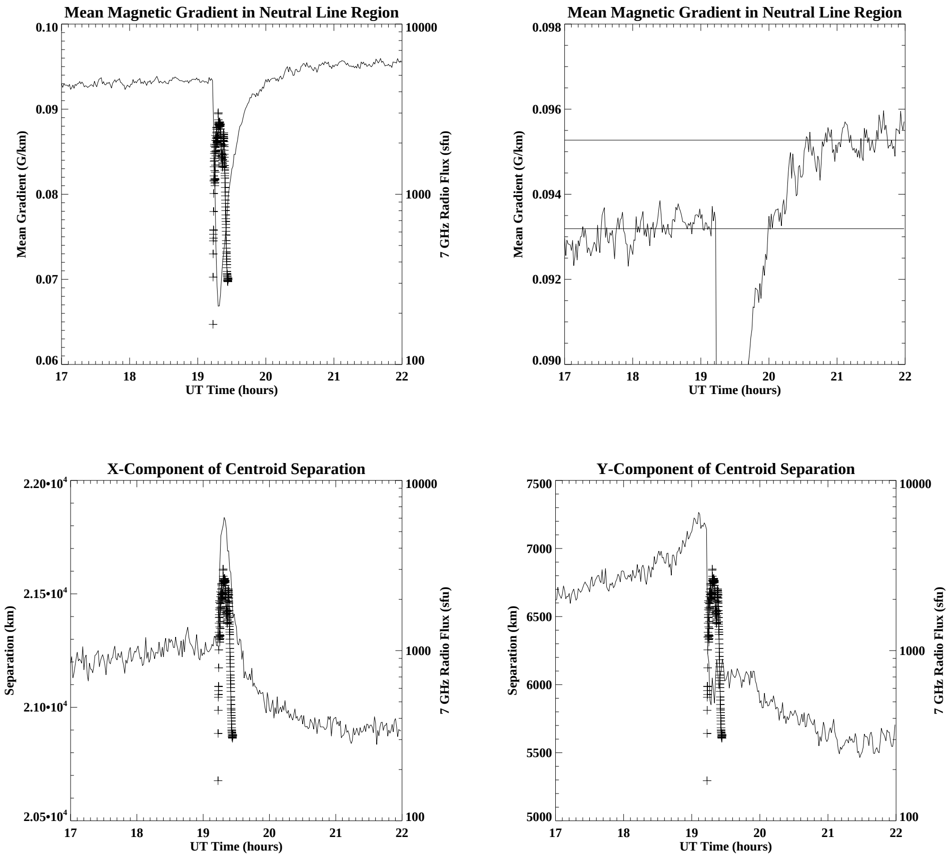

Figure 6. Evolution of magnetic gradient along the flaring neutral line and apparent sunspot motions associated with the X5.6 flare on 2001 April 6. Top panels show mean magnetic gradient along magnetic neutral line as a function of time. Bottom panels show the relative motion of sunspots of the opposite polarities following the flare. The flare timing is denoted by the Owens Valley 7GH microwave flux by "+" signs. In the direction normal to the neutral line (left), converging motion starts immediately following the flare; in the direction along the neutral line (right), an earthquake-like shear motion was found: before the flare, the two sunspots of opposite polarities in the two sides of the flaring neutral line have shearing motion. As soon as the flare occurred, the two spots slide back rapidly and reverse the direction of the relative motion (Stoltz, 2005).

Krall, K. R., Smith, J. B. J., Hagyard, M. J., West, E. A., & Cummings, N. P. 1982, Sol. Phys., 79, 59
Leka, K. D., & Barnes, G., 2003a, Ap.J., 595, 1277
Leka, K. D., & Barnes, G., 2003b, Ap.J., 595, 1296-1306
Li, H., Sakurai, T., Ichimoto, K. & UeNo, S., 2000a, PASJ, 52, 465
Li, H., Sakurai, T., Ichimoto, K. & UeNo, S., 2000b, PASJ, 52, 483
Liu, C., Deng, N., Liu, Y., Falconer, D., Goode, P. R., Denker, C., & Wang, H., 2005, Ap.J., 622, 722

Maeshiro et al., Ap.J., 2005, 620, 1069
McIntosh, P. S., 1990, Sol. Phys., 125, 251
Metcalf, Thomas R., Leka, K. D., & Mickey, D. L., 2005, Ap.J., Letters, 623, L53
Metcalf, T. R., Litao, J., McClymont, A. N., Canfield, R. C., & Uitenbroek, H. 1995, Ap.J., 439, 474
Molodenskii, M. M, 1969, Soviet Astronomy, 12, 585
Sawyer, C., Warwick, J. W., & Dennett, J. T., 1986, Boulder: Colorado Assoc. Univ. Press
Schrijver, C.J., DeRosa, M.L., Title, A.M. & Metcalf, 2005, Ap.J., 628, 501
Song, H., Yurchyshyn, v., Yang, G., Tang, C., Chen, W., Ma, J., Wang, H., 2006, Ap.J., submitted
Spirock, T. J., Yurchyshyn, V. B., & Wang, H., 2002, Ap. J., 572, 1072
Stoltz, J., 2005, Masters Thesis, New Jersey Institute of Technology
Sudol, J.J. & Harvey, J.W., 2005, Ap.J., 635, 647
Tang, F & Wang, H., 1993, Sol. Phys. 132, 247
Tanaka, K., 1991, Sol. Phys., 136, 133
Wang, H., Ewell, M. W., Zirin, H. & Ai, G., 1994, Ap.J., 424, 436
Wang, H., Qiu, J., Jing, J. & Zhang, H., 2003, Ap.J., 593, 564
Wang, H., Qiu, J., Jing, J., Spirock, T. J. & Yurchyshyn, V., 2004, Ap.J., 605, 931
Wang, H., Song, H., J.ing, J., Yurchyshyn, V., Deng, Y., Zhang, H., Falconer, D., & Jing, L., 2006, Ap. J., submitted
Wang, J., Shi, Z., Wang, H. & Lü, Y., 1996, Ap.J., 456, 861
Wang, T., Xu, A. & Zhang, H., 1994, Sol. Phys., 155, 99
Yang, G., Xu, Y., Cao, W., Wang, H., Denker, C., & Rimmele, T. R., 2004, Ap.J. Letters, 617, L151
Yurchyshyn, V. B., Wang, H., Abramenko, V., Spirock, T. J., & Krucker, S., 2004, Ap.J., 605, 546
Zhang, H., Ai, G., Yan, X., Li, W., & Liu, Y. 1994, Ap.J., 423, 828
Zirin, H., 1983, Ap.J., 274, 900
Zirin, H., & Liggett, M. A., 1987, Sol. Phys., 113, 267
Zirin, H. & Marquette, W., 1991, Sol. Phys., 131, 149
Zirin, H., & Wang H., 1993, Nature, 363,426